Boosting methane selectivity in CO_2 electroreduction via rational modulation of Cu^0-Cu^+ sites in Cu/Cu_2O composite

Jia Yao [a], Qixiang Huang [b], Hanqi Li [b], Zhaofu Zhang [a], Zhuo Jiang [b,*], Yuzheng Guo [c,*]

[a] *School of Integrated Circuits, Wuhan University, Wuhan 430072, China*

[b] *School of Electrical Engineering and Automation, Wuhan University, Wuhan 430072, China*

[c] *School of Power and Mechanical Engineering, Wuhan University, Wuhan 430072, China.*

* Corresponding authors.

E-mail addresses: yguo@whu.edu.cn (Y. Guo), zhuojiang@whu.edu.cn (Z. Jiang).

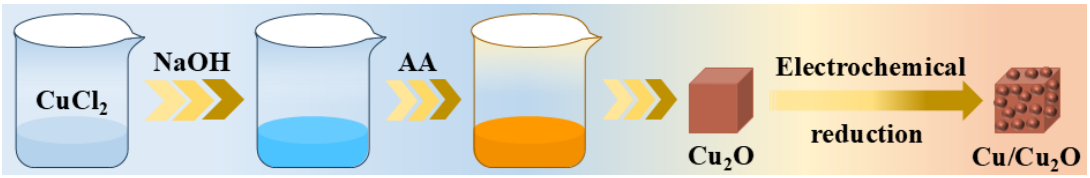

Fig. S1 Schematic illustration of the synthesis of Cu_2O and Cu/Cu_2O nanocubes.

Table S1

Synthesis conditions for size control of cubic Cu_2O particles.

Entry	Amount of $CuCl_2 \cdot 2H_2O$ / mmol	NaOH addition temperature / ℃	AA reduction temperature / ℃	Aging temperature / ℃	Aging duration / h	Particle size / nm
1	1.0	25	25	25	1	239 ± 7
2	1.0	25	25	55	3	279 ± 7
3	1.0	25	55	55	3	304 ± 9
4	2.0	25	25	55	3	310 ± 16
5	2.0	25	55	55	3	343 ± 24
6	0.5	25	55	55	3	475 ± 19
7	0.5	35	55	55	3	799 ± 39
8	0.2	55	55	55	3	890 ± 42
9	0.5	55	55	55	3	964 ± 29
10	0.5	55	25	55	3	1021 ± 70
11	1.0	55	25	55	3	1089 ± 56
12	1.0	55	55	55	3	1240 ± 43
13	2.0	55	55	55	3	1482 ± 63
14	2.0	55	25	55	3	1630 ± 48

Each reaction was conducted in 100 mL of deionized water under continuous stirring at 500 rpm. NaOH and ascorbic acid (AA) solutions were added dropwise (0.5 mL/min). SEM was used to characterize the morphology and size of cubic Cu_2O particles.

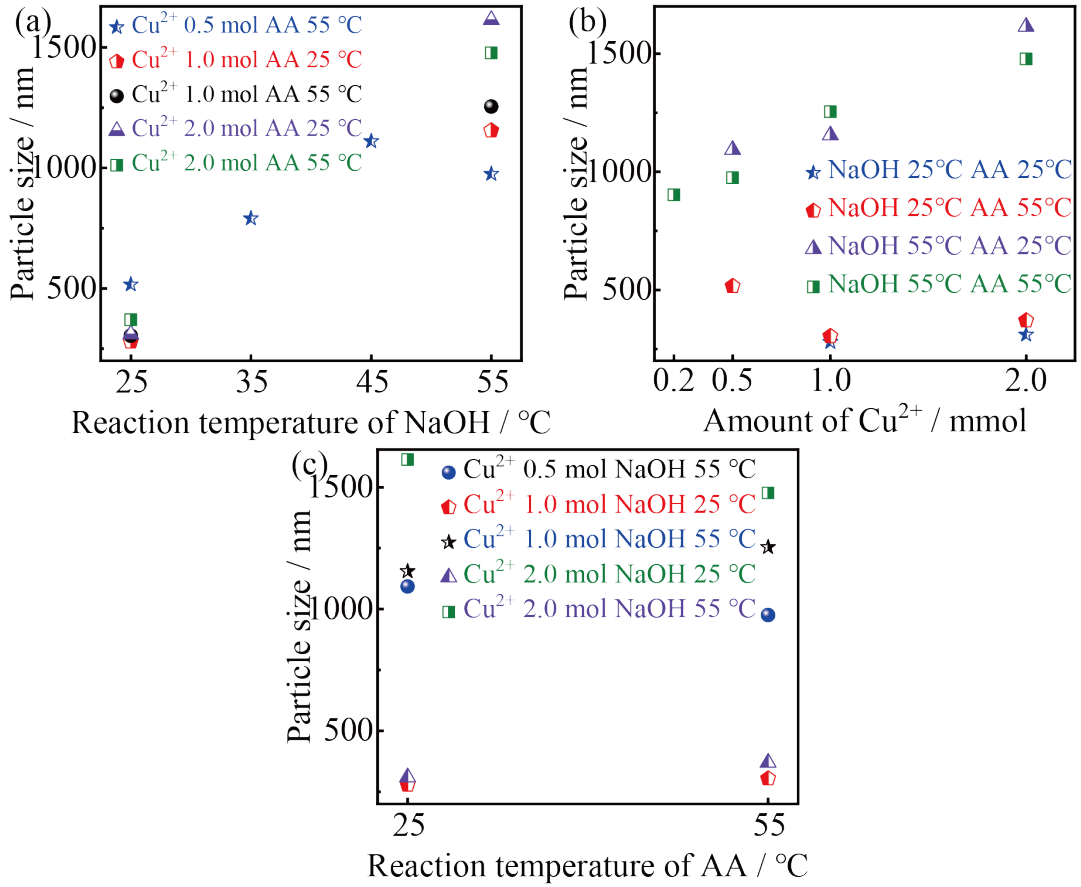

Fig. S2 (a-c) Effect of reaction parameters on the size of cubic Cu_2O particles. (a) NaOH reaction temperature, (b) Cu^{2+} concentration, and (c) ascorbic acid (AA) reaction temperature.

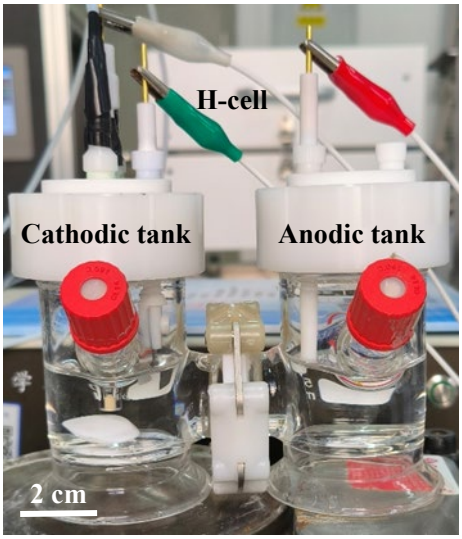

Fig. S3 Schematic of the CO_2RR electrolysis system.

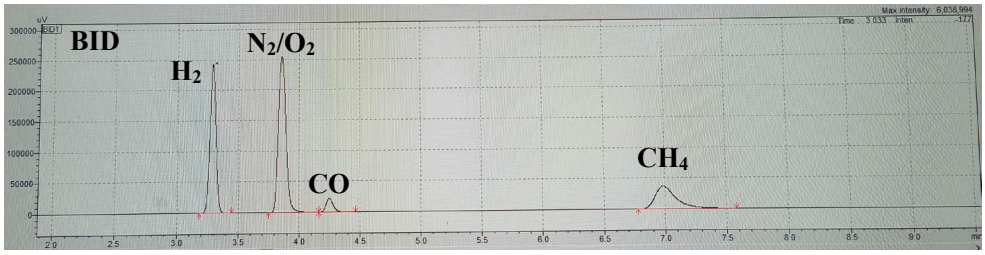

Fig. S4 Representative gas chromatogram of H_2, CO, and CH_4 detected by barrier ionization detector (BID).

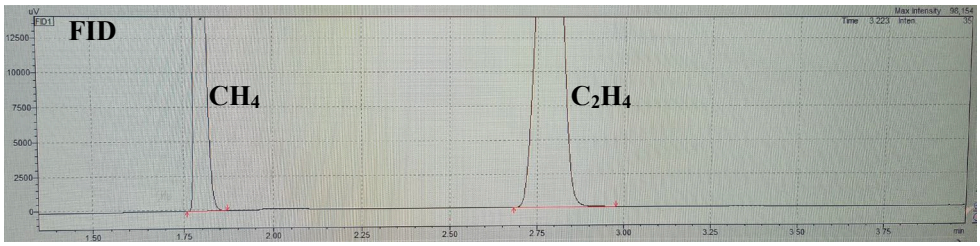

Fig. S5 Representative gas chromatographic of CH_4 and C_2H_4 detected by flame ionization detector (FID).

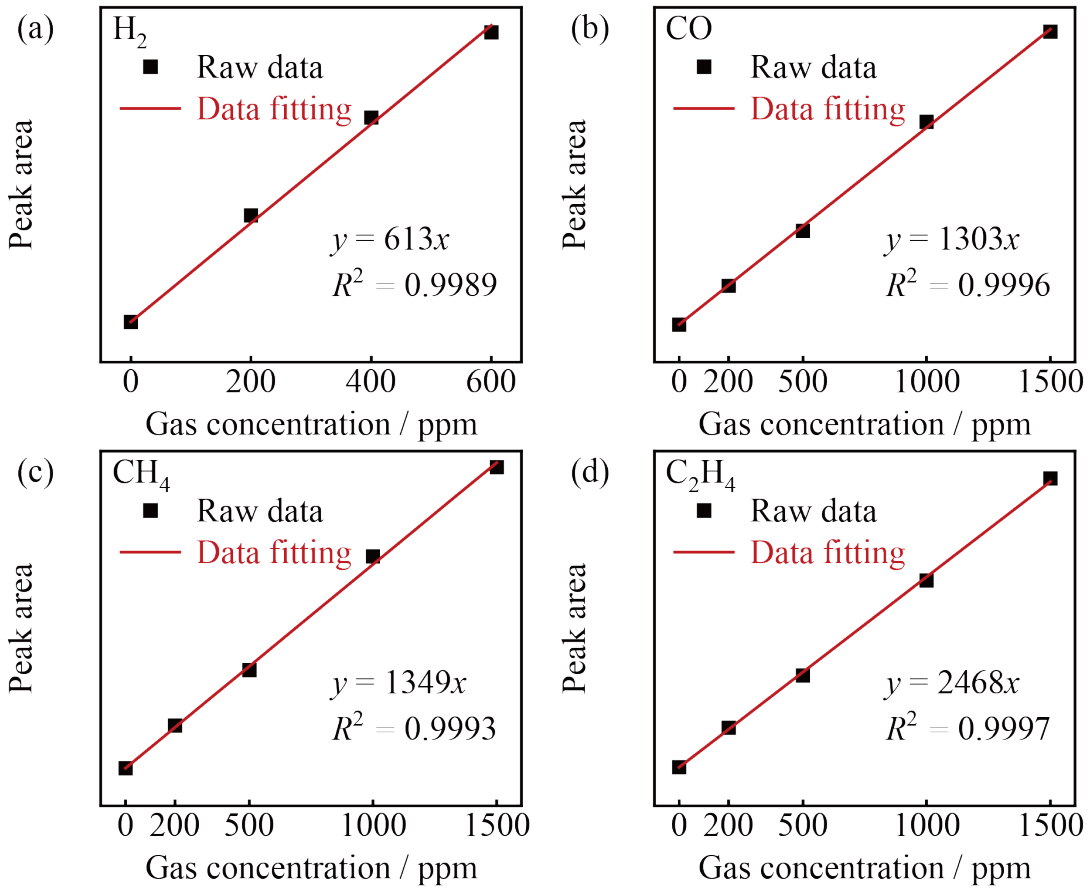

Fig. S6 (a-d) Gas chromatography calibration curves for H_2 (a), CO (b), CH_4 (c), and C_2H_4 (d).

Standard curves were generated by plotting peak areas against known gas concentrations, with linear regression yielding correlation coefficients ($R^2 >$ 0.998) for all analytes.

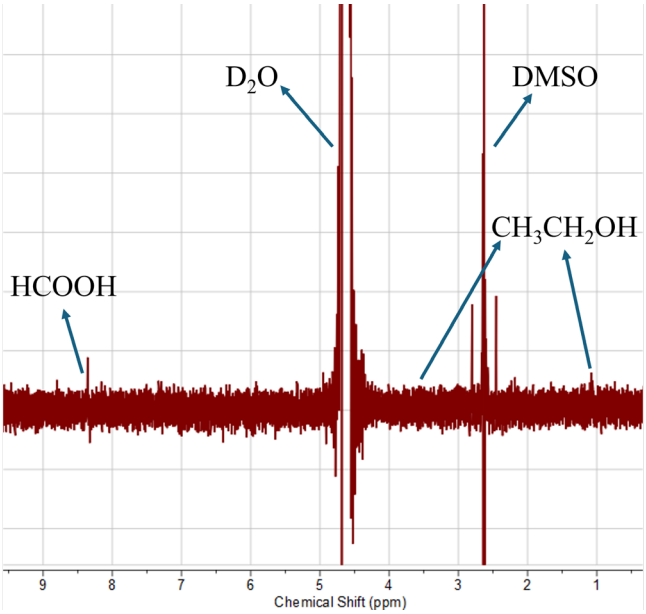

Fig. S7 A typical ^{1}H NMR spectrum of the detected liquid products.

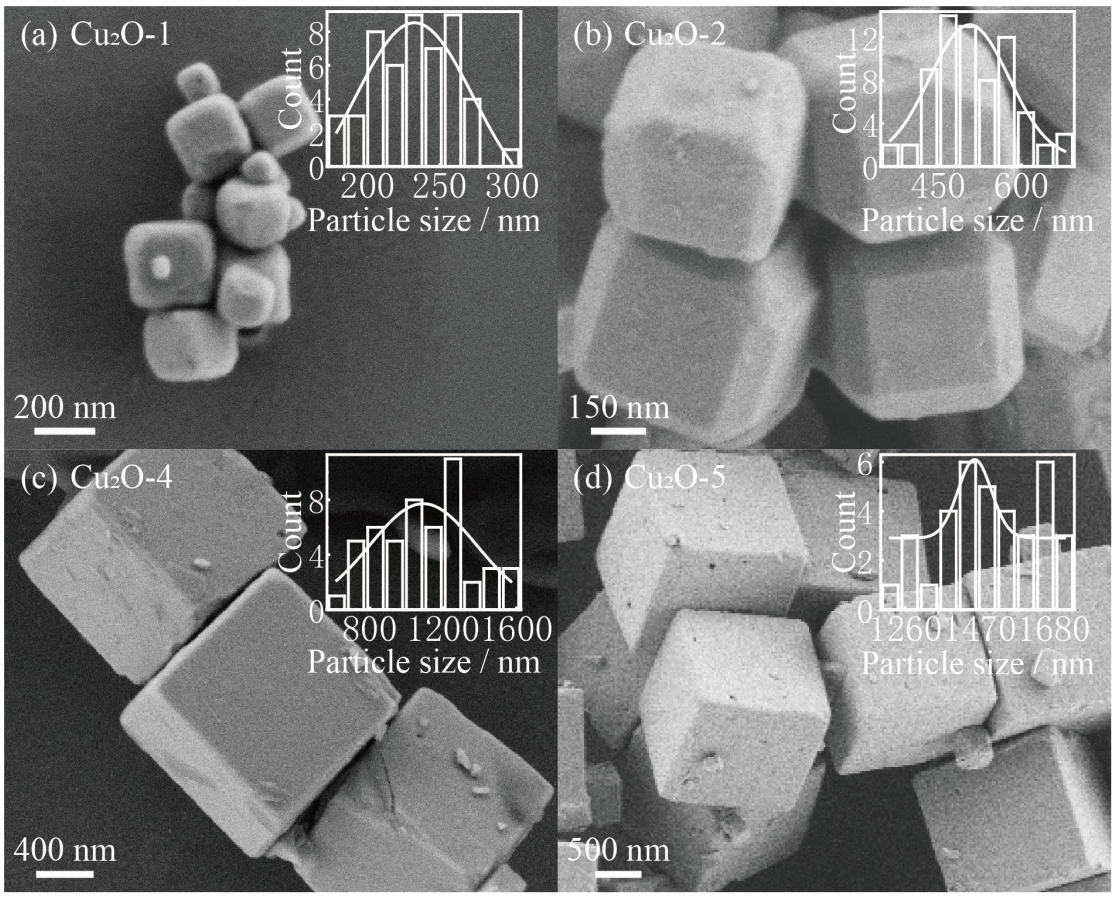

Fig. S8 (a-d) FESEM images of (a) Cu_2O-1, (b) Cu_2O-2, (c) Cu_2O-4, and (d) Cu_2O-5, with inset particle size distribution histograms.

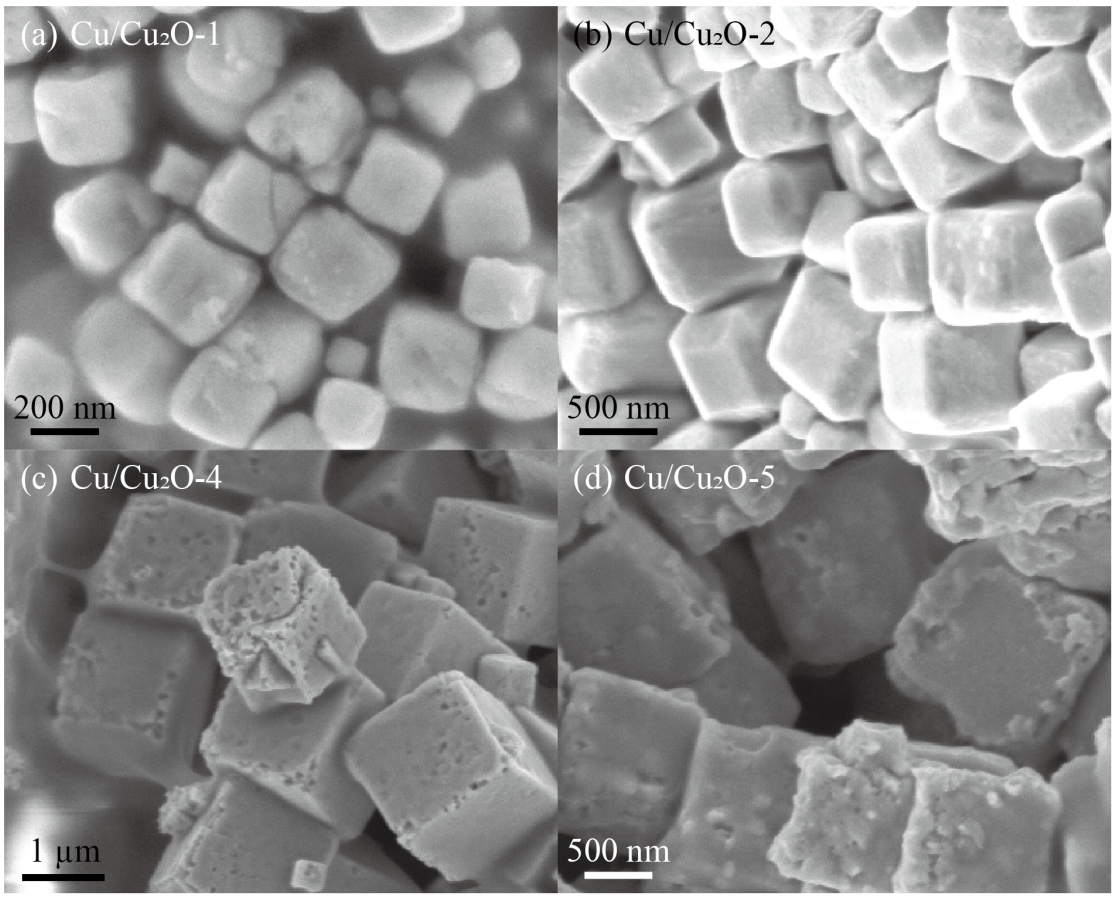

Fig. S9 (a-d) FESEM images of (a) Cu/Cu_2O-1, (b) Cu/Cu_2O-2, (c) Cu/Cu_2O-4, and (d) Cu/Cu_2O-5.

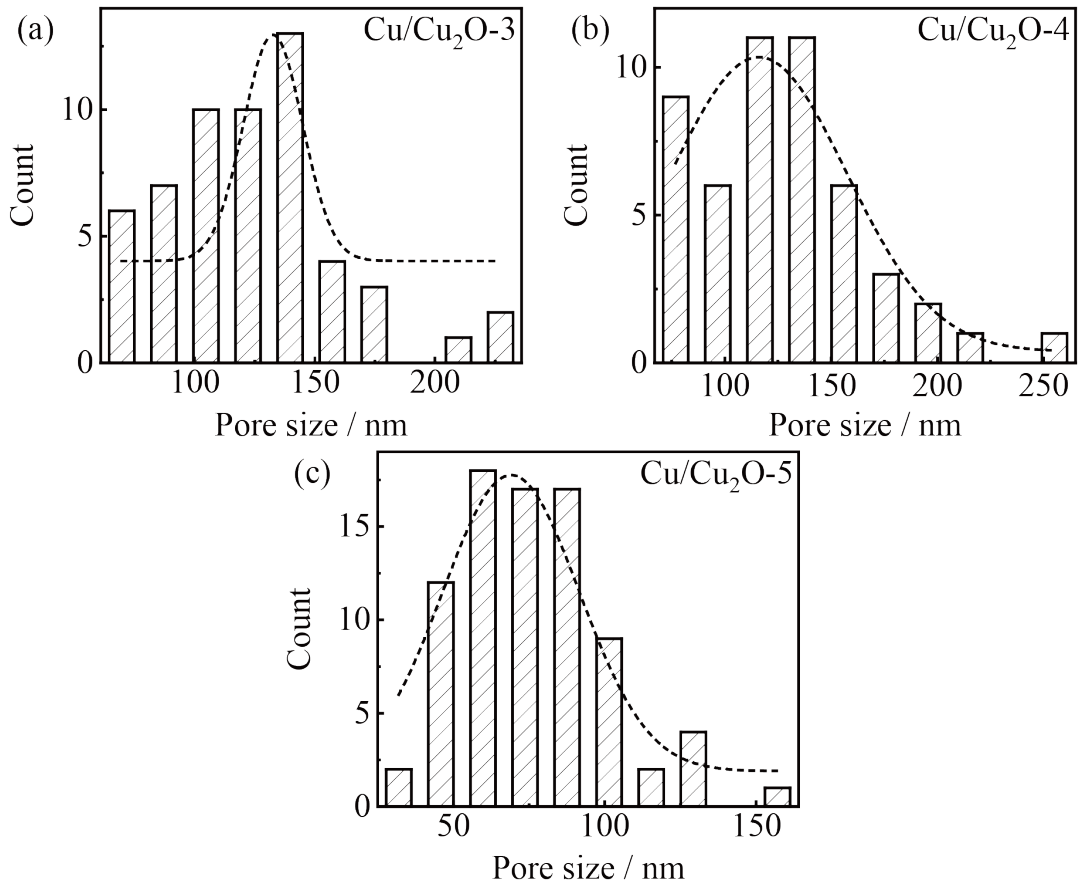

Fig. S10 (a-c) Pore size distribution histograms derived from the FESEM images of the cube-shaped surfaces for (a) Cu/Cu_2O-3, (b) Cu/Cu_2O-4, and (c) Cu/Cu_2O-5.

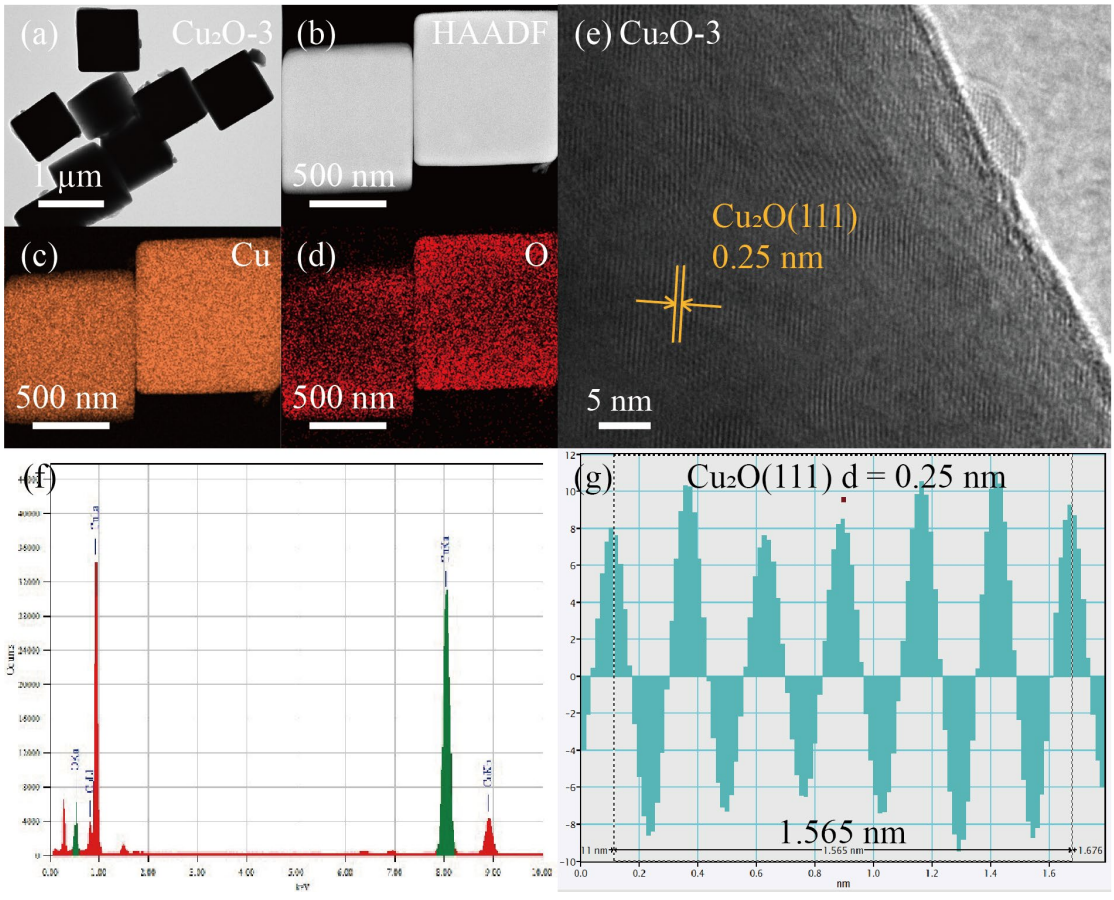

Fig. S11 (a-f) TEM (a), HRTEM (e), and EDS (f) results of Cu_2O-3. (b) HAADF image with corresponding Cu (c) and O (d) elemental mappings. (g) Lattice fringe spacing of 0.25 nm in the orange dashed area (e) corresponds to Cu_2O.

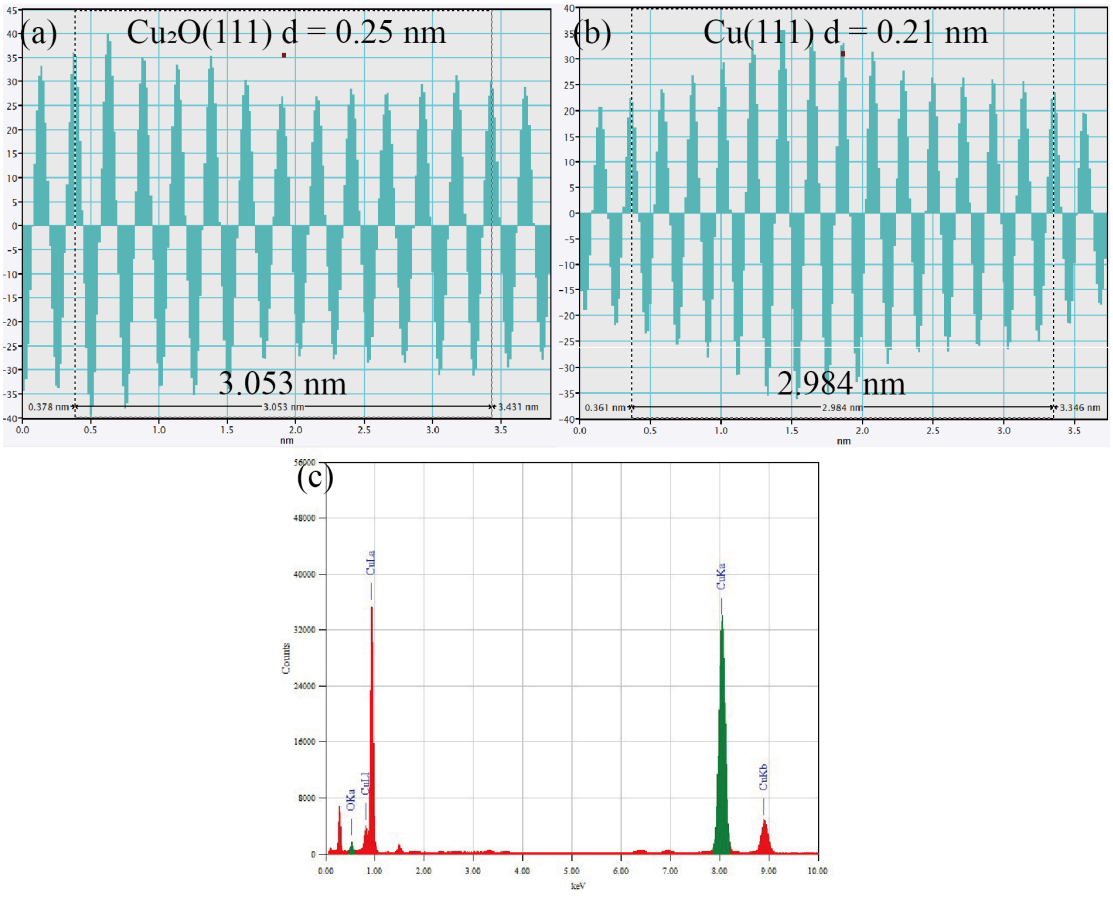

Fig. S12 (a,b) HRTEM image of Cu/Cu_2O-3 (Fig. 1i) shows interplanar spacings of 0.25 nm (a) and 0.21 nm (b) in the orange and white dashed regions, consistent with d-spacing of Cu_2O and Cu, respectively. (c) EDS result of Cu/Cu_2O-3.

Table S2

Atomic ratios of copper and oxygen in Cu_2O-3 and Cu/Cu_2O-3 quantified by TEM-EDS.

Sample	Cu / at%	O / at%
Cu_2O-3	78.91	21.09
Cu/Cu_2O-3	94.84	5.16

Table S3

XRD-derived mass fractions of Cu and Cu_2O, and atomic ratios of Cu^0/Cu^+ in Cu/Cu_2O catalysts.

Sample	Cu / wt%	Cu_2O / wt%	Cu^0 / at%	Cu^+ / at%
Cu/Cu_2O-1	9.5	90.5	10.7	89.3
Cu/Cu_2O-2	13.6	86.4	15.6	84.4
Cu/Cu_2O-3	20.6	79.4	22.6	77.4
Cu/Cu_2O-4	18.0	82.0	20.0	80.0
Cu/Cu_2O-5	13.5	86.5	15.5	84.5

Cu and Cu_2O contents were quantified using the relative intensity ratio (RIR) method.[1] Eq. (S1) was used with RIR values from PDF cards: Cu (JCPDS No. 04-0836, RIR = 4.07) and Cu_2O (JCPDS

No. 05-0667, RIR = 3.12). Here, W_{Cu} and W_{Cu_2O} are mass fractions ($W_{Cu} + W_{Cu_2O} = 1$), and I_{Cu} and I_{Cu_2O} are integrated intensities of the strongest peaks (Cu (111) and Cu_2O (111), respectively, Fig. 1b).

$$W_{Cu} = \frac{I_{Cu}}{I_{Cu}+(I_{Cu_2O}/(RIR_{Cu_2O}/RIR_{Cu}))} \quad \text{(S1)}$$

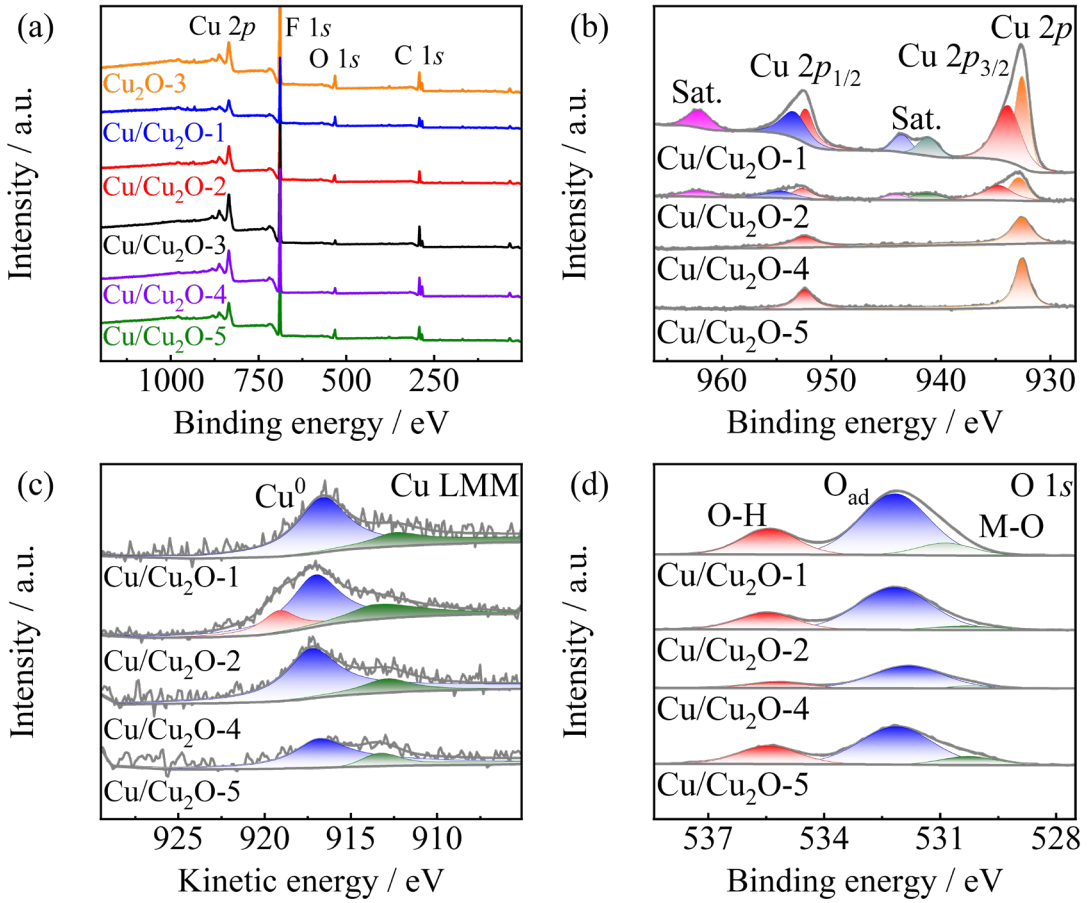

Fig. S13 (a-d) XPS spectra analysis: (a) survey spectra, and high-resolution (b) Cu 2*p*, (c) Cu LMM, and (d) O 1*s* spectra of Cu_2O-3 and Cu/Cu_2O catalysts.

Table S4

Atomic percentages of Cu^0, Cu^+, and M-O in Cu_2O-3 and Cu/Cu_2O catalysts quantified by XPS.

Sample	Cu^0 / at%	Cu^+ / at%	Cu^0 / Cu^+ ratio	M-O / at%
Cu_2O-3	/	81.23	/	23.85
Cu/Cu_2O-1	72.20	27.80	2.60	11.04
Cu/Cu_2O-2	69.27	15.30	4.50	5.81
Cu/Cu_2O-3	81.48	8.42	9.68	3.90
Cu/Cu_2O-4	82.17	17.83	4.60	4.96
Cu/Cu_2O-5	74.74	25.26	2.96	10.65

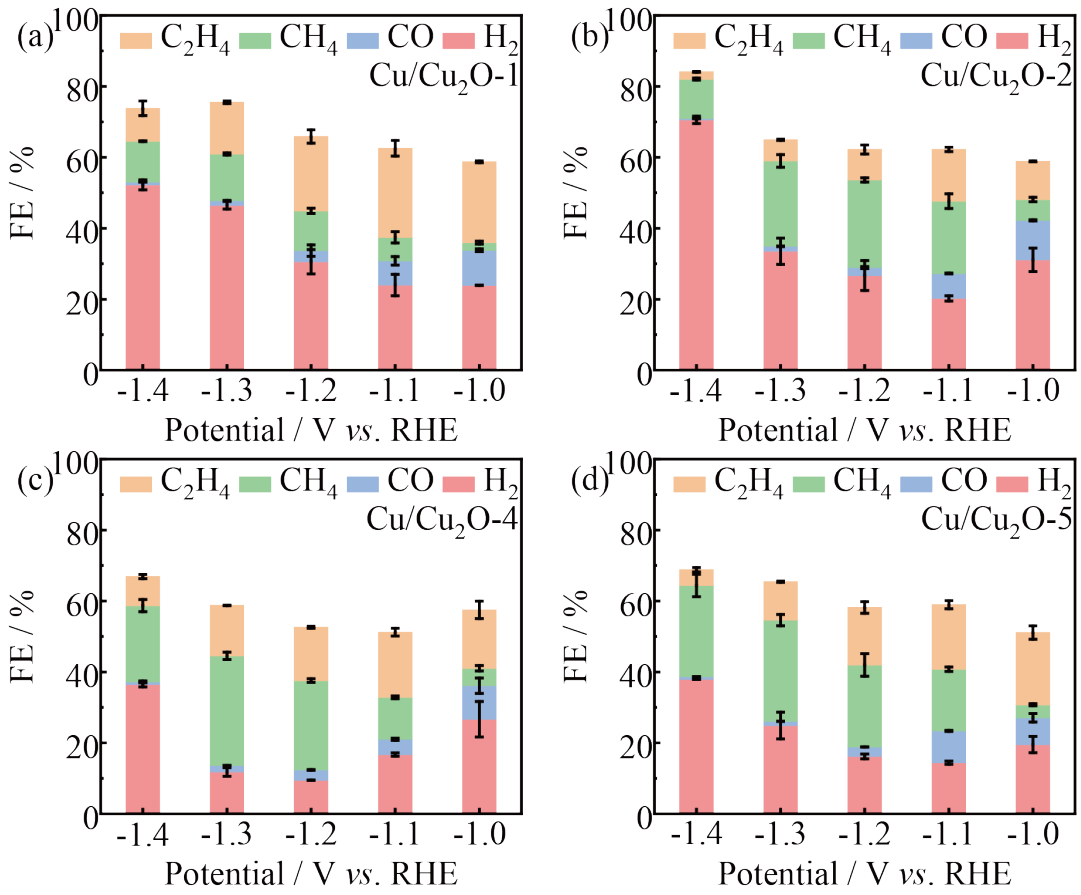

77

78 **Fig. S14** (a-d) Faradaic efficiency plots of (a) Cu/Cu_2O-1, (b) Cu/Cu_2O-2, (c) Cu/Cu_2O-4, and (d)
79 Cu/Cu_2O-5 in CO_2-saturated 0.2 M KCl + 0.1 M $KHCO_3$ at different potentials.

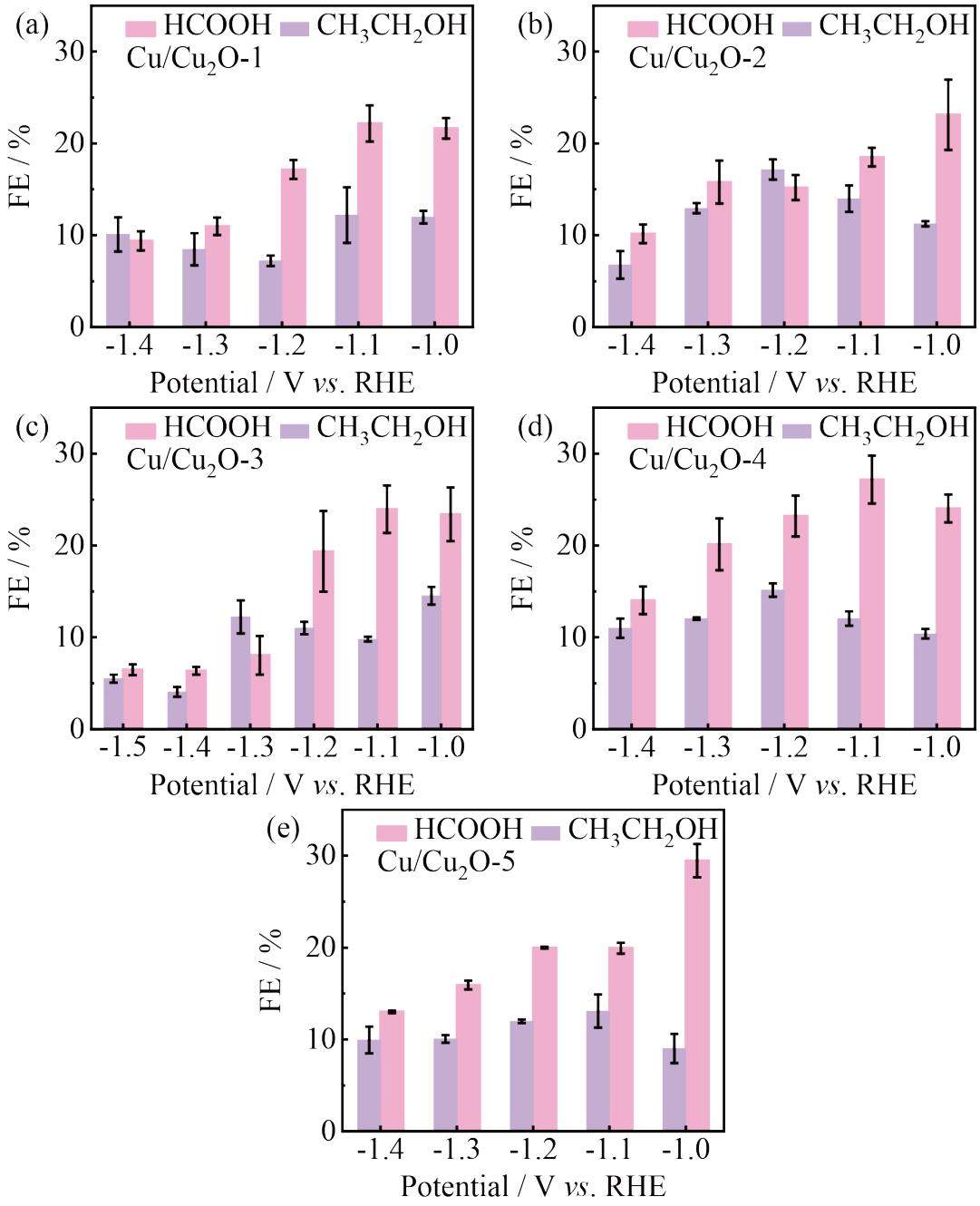

Fig. S15 (a-e) Faradaic efficiency plots of liquid products for (a) Cu/Cu_2O-1, (b) Cu/Cu_2O-2, (c) Cu/Cu_2O-3, (d) Cu/Cu_2O-4 and (e) Cu/Cu_2O-5 in CO_2-saturated 0.2 M KCl + 0.1 M $KHCO_3$ at different potentials.

Table S5

State-of-the-art copper-based catalysts for electrochemical CO_2 conversion to CH_4.

Electrocatalyst	Electrolyte	FE(CH_4) / %	*E* / V *vs.* RHE	*j* / mA cm^{-2}	Ref.
Cu_2O-CeO_2-2	0.1 M $KHCO_3$	35	-1.3	4	2
Ag-Cu_2O-3	0.1 M $KHCO_3$	55	-1.3	7	3
Cu@C	0.1 M $KHCO_3$	56	-1.3	11	4
Cu_2O-Cu	0.5 M KCl+0.5 M $NaHCO_3$	37	-1.3	60	5
Cu-N_4/Cu/Cu_2O	0.1 M KCl+0.1 M $KHCO_3$	30	-1.3	8	6
CeO_2/Cu_2O-C dots	0.5 M $KHCO_3$	38	-1.3	5	7
Cu/Si	0.1 M $KHCO_3$	71	-2.2	23	8
CuSbF	0.5 M $KHCO_3$	65	-1.3	95	9
Cu foil-PANI	0.1 M KCl+0.1 M $KHCO_3$	30	-1.3	10	10
Cu-CeO_2	0.1 M $KHCO_3$	32	-1.3	12	11
CNA/Cu_2O/Pd2	0.1 M $KHCO_3$	1	-1.2	15	12
CuO+Ni-surface	0.1 M $KHCO_3$	5	-1.6	8	13
CuR/Ag	0.1 M $KHCO_3$	8	-1.8	26	14
Cu/Cu_2O@NC-2	0.1 M $KHCO_3$	30	-1.5	30	15
$CuPz_2$-Act-30	0.1 M KCl	10	-0.8	10	16
p-Cu@Cu_2O	0.1 M $KHCO_3$	10	-1.3	15	17
Pd_{40}/Cu_2O-Cu	0.5 M $NaHCO_3$	30	-0.65	20	18
Cu_2O/Cu	0.1 M $KHCO_3$	3	-0.7	10	19
SW Cu_2O	0.1 M KCl	5	-1.6	120	20
CuO-ER	0.1 M $KHCO_3$	8	-1.5	11	21
Cu-I	0.2 M K_2SO_4	40	-1.4	15	22
c-Cu_2O	0.1 M $KHCO_3$	20	-1.3	8	23
Cu NCs-OCP200	0.1 M $KHCO_3$	32	-1.3	3	24
Au@Cu_2O-M-10	0.1 M KCl	66	-1.3	30	25
Cu/Cu_2O-3	0.2 M KCl+0.1 M $KHCO_3$	43	-1.3	15	This work

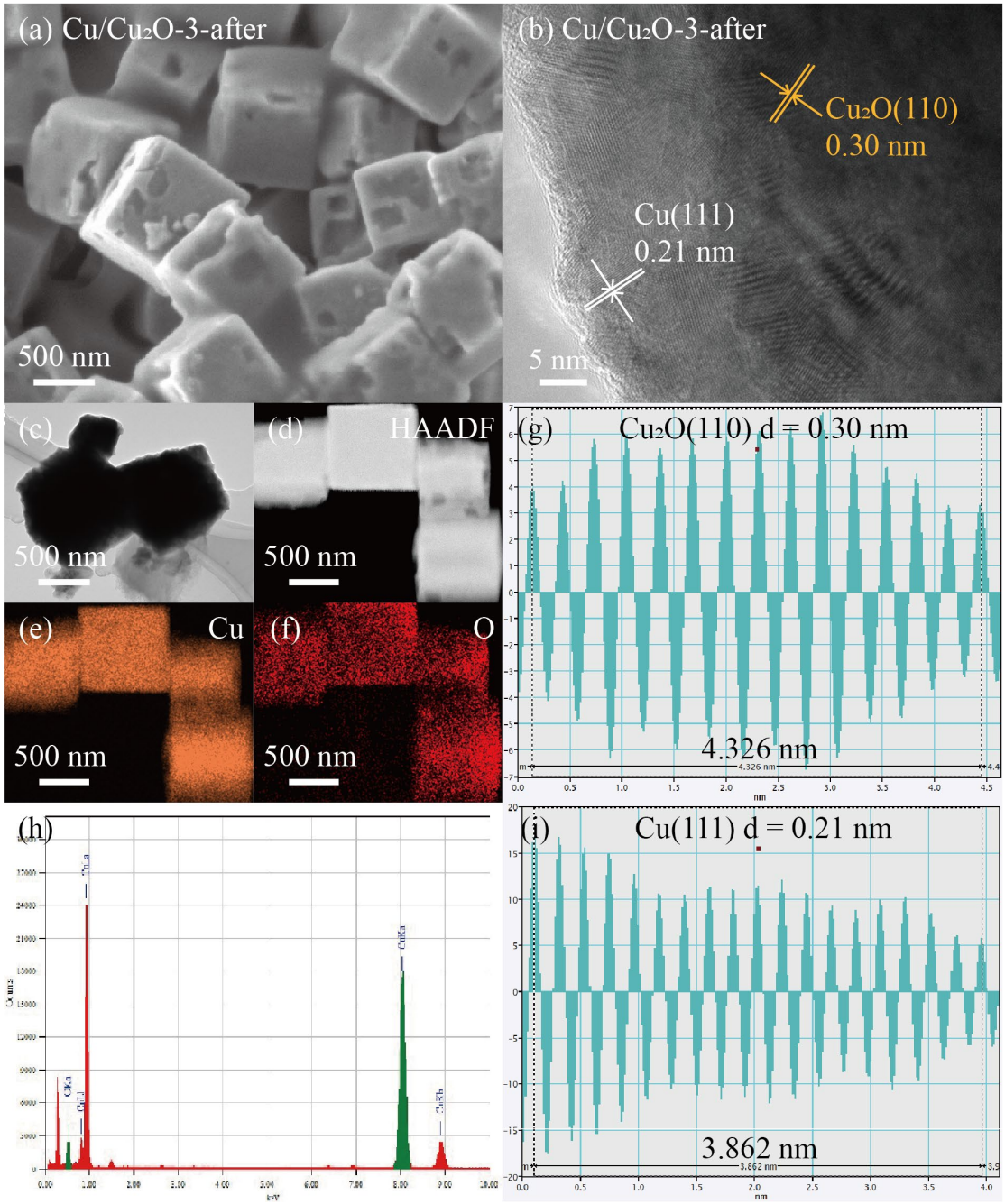

Fig. S16 (a-c) FESEM (a), HRTEM (b), and TEM (c) images of Cu/Cu_2O-3 after stability testing in CO_2-saturated 0.2 M KCl + 0.1 M $KHCO_3$. (d) HAADF image with corresponding Cu (e) and O (f) elemental mappings of post-test Cu/Cu_2O-3. (g,i) HRTEM image shows interplanar spacings of 0.30 nm (g) and 0.21 nm (i) in dashed regions, matching d-spacings of Cu_2O and Cu. (h) EDS result of post-test Cu/Cu_2O-3.

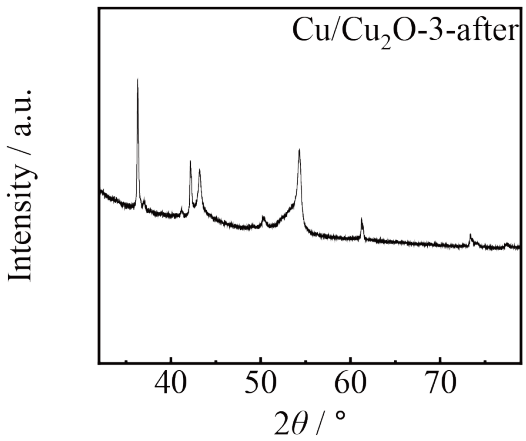

100

101 **Fig. S17** Post-stability XRD pattern of Cu/Cu_2O-3 after stability testing in CO_2-saturated 0.2 M KCl
102 + 0.1 M $KHCO_3$.
103

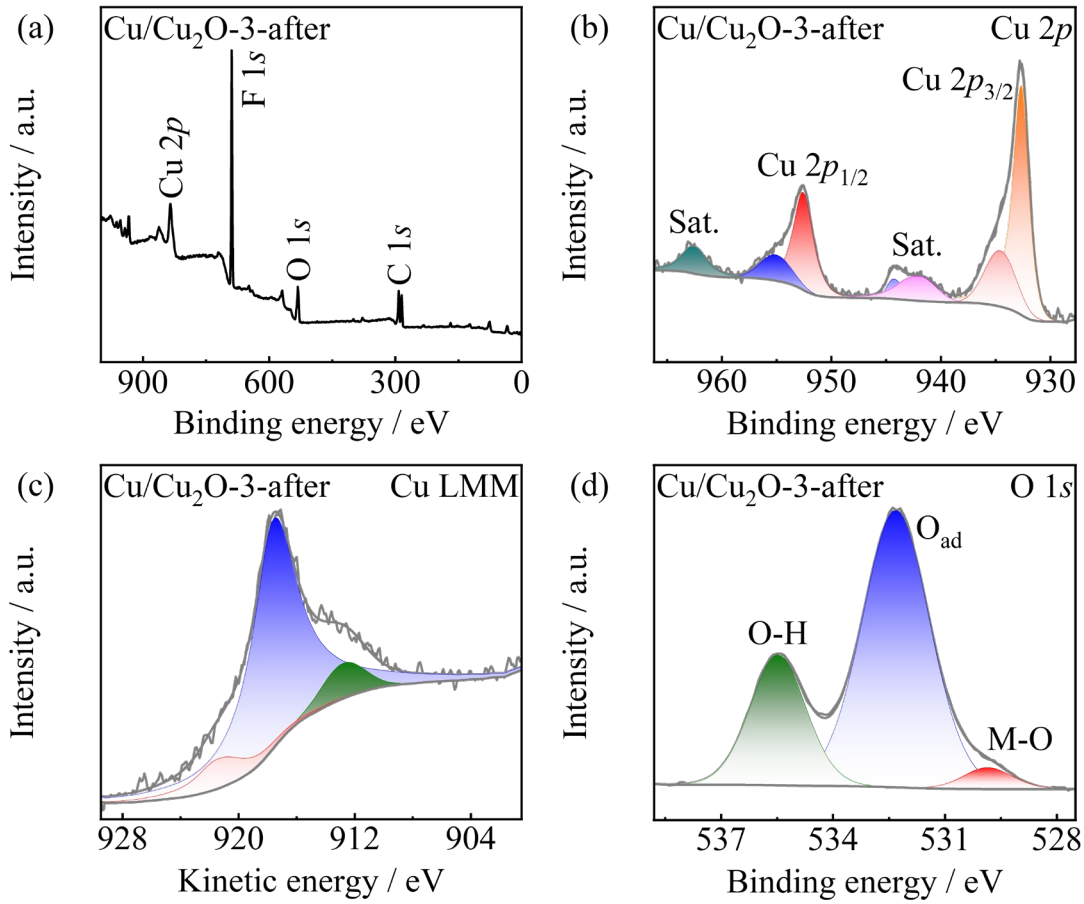

104

105

106 **Fig. S18** (a-d) XPS spectra of post-stability Cu/Cu_2O-3: (a) survey spectra, and high-resolution (b)
107 Cu 2*p*, (c) Cu LMM, and (d) O 1*s* spectra after testing in CO_2-saturated 0.2 M KCl + 0.1 M $KHCO_3$.

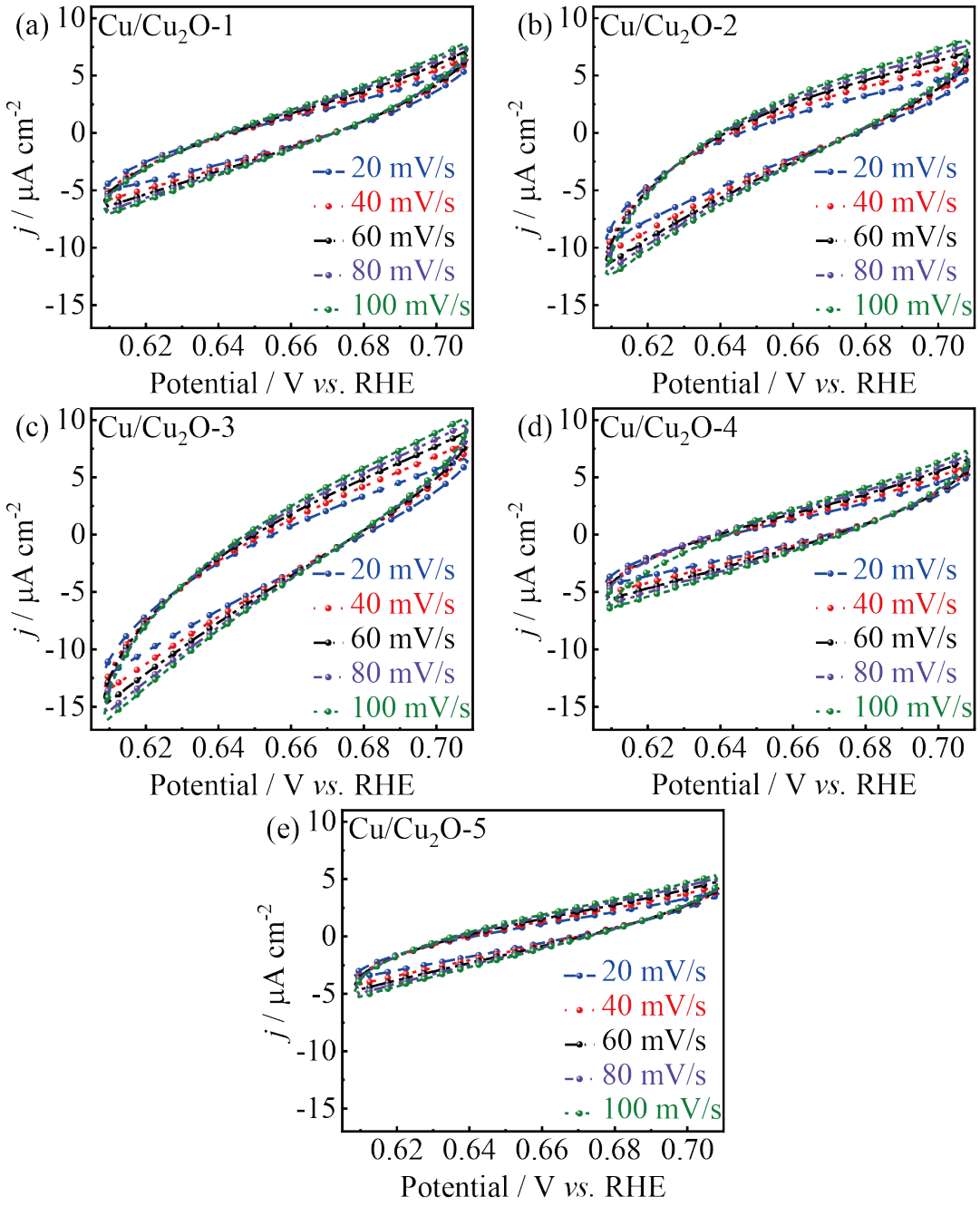

Fig. S19 (a-e) CV curves of (a) Cu/Cu_2O-1, (b) Cu/Cu_2O-2, (c) Cu/Cu_2O-3, (d) Cu/Cu_2O-4, and (e) Cu/Cu_2O-5 in CO_2-saturated 0.2 M KCl + 0.1 M $KHCO_3$ electrolyte at scan rates of 20-100 mV/s.

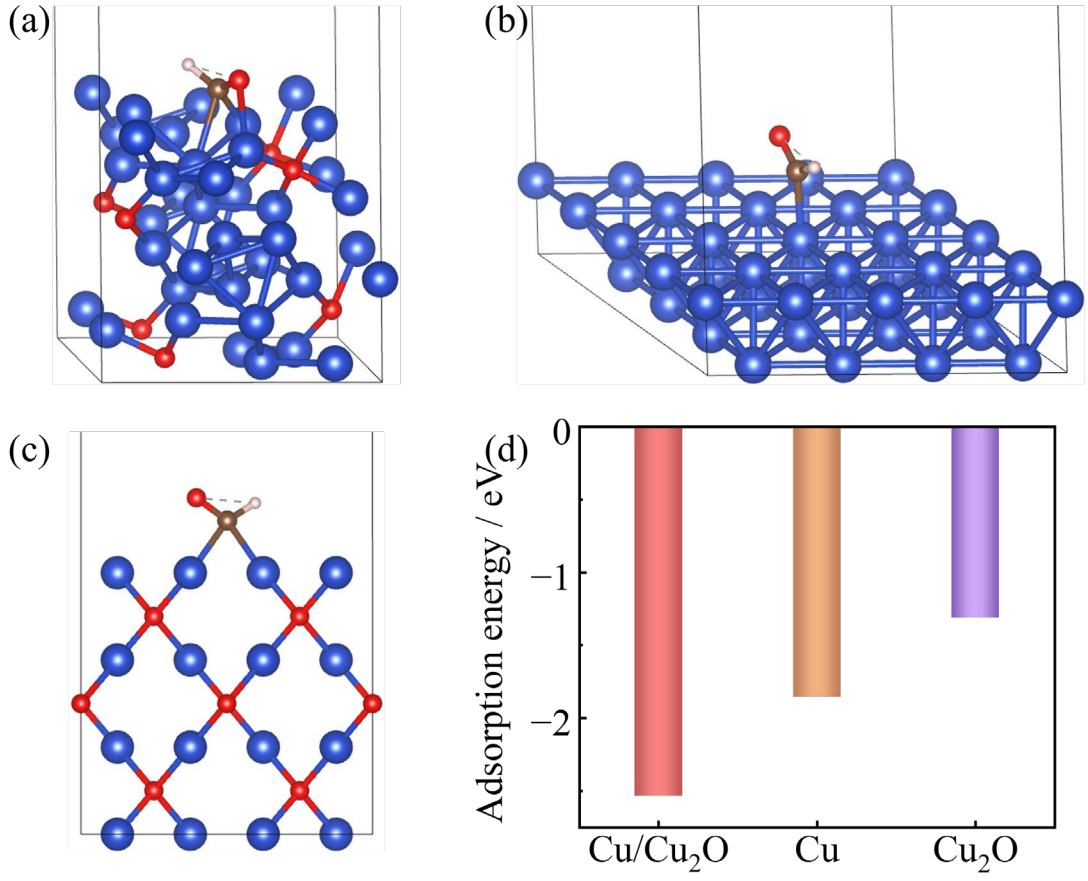

Fig. S20 (a-c) Adsorption models of the *CHO species on (a) Cu(111)/Cu_2O(100) interface, (b) Cu(111), and (c) Cu_2O(100). (In which, copper, oxygen, carbon, and hydrogen atoms are represented by blue, red, brown, and white spheres, respectively.) (d) The calculated adsorption energy of *CHO species on Cu/Cu_2O interface, Cu and Cu_2O models.

References

1 J. Li, S.-X. Guo, F. Li, F. Li, X. Zhang, J. Ma, D. R. MacFarlane, A. M. Bond and J. Zhang, *ChemSusChem*, 2019, **12**, 4471-4479.

2 L. Yu, L. Zhou, Q. Guo, H. Zhang, X. Xiao, R. Zhao, Z. Yan and Y. Zhang, *Int. J. Hydrog. Energy*, 2025, **132**, 10-17.

3 M. Sun, L. Zhang, F. Tian, J. Li, Y. Lei, H. Zhang, L. Han, Z. Guo, Y. Gao, F. Liu, Y. Wang and L. Wang, *J. Energy Chem.*, 2024, **88**, 521-531.

4 F. Li, H. Tariq, H. Yang, Y. Cao, T. Zhou and G. Wang, *ACS Catal.*, 2024, **14**, 15088-15095.

5 S. Xu, L. Yang, C. Wang, L. Pan, J. Zhang, Y. Wang and H. Zhong, *J. Mater. Chem. C*, 2025, **13**,

6933-6943.

6 W. Xiong, D. Si, J. Yi, Y. Huang, H. Li and R. Cao, *Appl. Catal. B-Environ. Energy*, 2022, **314**, 121498.

7 X. Yan, J. Li, H. Si, H. Xu, H. Huang, Y. Liu and Z. Kang, *Inorg. Chem. Front.*, 2025, **12**, 2024-2035.

8 J. Song, H. Sun, S. Yao, Z. Liu, M. Lv, F. Li, Z. Lv, X. Hu, H. Wang and L. Liu, *Small*, 2025, **21**, 2411491.

9 K. Wan, X. Jiang, X.-P. Li, Z. Cao, Z.-H. He, W. Wang, H. Wang, X. Lai and Z.-T. Liu, *Green Chem.*, 2025, **27**, 6027-6038.

10 Y.-T. Wen, W.-F. Xiong, D.-H. Si, H.-F. Li and R. Cao, *Inorg. Chem. Front.*, 2025, **12**, 5811-5818.

11 L. Xue, Y. Zhao, Y. Qi, G. Fan, S. Zeng, Y. Qin and B. Zhang, *J. Energy Chem.*, 2025, **107**, 759-767.

12 P. Uthirakumar, D. Kim, V. Dao, C. Kai, C. Yun, Y. J. Jang and I.-H. Lee, *Environ. Res.*, 2025, **265**, 120423.

13 M. Li, S. Kuang, Y. Jin, H. Chi, S. Zhang and X. Ma, *Chem. Eng. J.*, 2025, **506**, 160048.

14 P. Uthirakumar, H. Son, V. Dao, Y. Lee, S. Yadav and I.-H. Lee, *J. Environ. Chem. Eng.*, 2024, **12**, 112442.

15 F. Li, H. Tariq, H. Yang, Y. Cao, T. Zhou and G. Wang, *ACS Catal.*, 2024, **14**, 15088-15095.

16 C. Liu, X.-D. Zhang, J.-M. Huang, M.-X. Guan, M. Xu and Z.-Y. Gu, *ACS Catal.* 2022, **12**, 15230-15240.

17 M. Ye, T. Shao, J. Liu, C. Li, B. Song and S. Liu, *Appl. Surf. Sci.*, 2023, **622**, 156981.

18 J. Li, S.-X. Guo, F. Li, F. Li, X. Zhang, J. Ma, D. R. MacFarlane, A. M. Bond and J. Zhang, *ChemSusChem*, 2019, **12**, 4471-4479.

19 Z. Yan, P. Gao, Z. Li, Y. Zhang, C. Hu, D. Cao and D. Cheng, *Small*, 2025, **21**, 2500950.

20 S. Wang, D. Wang, B. Tian, X. Gao, L. Han, Y. Zhong, S. Song, Z. Wang, Y. Li, J. Gui, M. G. Sendeku, Y. Zhang, Y. Kuang and X. Sun, *Sci. China Mater.*, 2023, **66**, 1801-1809.

21 Y. Qu, W. Zheng, P. Wang, H. Huang, M. Huang, L. Hu, H. Wang and Q. Chen, *J. Colloid Interface Sci.*, 2023, **645**, 735-742.

22 Y. Jiang, H. He, D. Xia, H. Zhang, S. Tan, L. Luo, Y. Kong, L. Deng and Y.-N. Liu, *Green Chem.*, 2025, **27**, 9737-9745.

23 B. Deng, M. Huang, K. Li, X. Zhao, Q. Geng, S. Chen, H. Xie, X. Dong, H. Wang and F. Dong, *Angew. Chem. Int. Ed.*, 2022, **61**, e202114080.

24 S. Popovic, M. A. Nazrulla, P. Sket, K. M. Kamal, B. Likozar, L. Suhadolnik, L. Pavko, A. K. Surca, M. Bele and N. Hodnik, *Electrochim. Acta*, 2022, **436**, 141458.

25 Z. Zhang, H. Guo, S. Li, S. Gao, X. Wang, M. Li, W. Yan and H. Xu, *Nat. Commun.*, 2025, **16**, 7559.